Theoretical studies of a nanoparticle bridge platform for molecular electronics measurements

Henrik Löfås

Licentiate Thesis in Physics
Department of Physics and Astronomy

2011

UPPSALA
UNIVERSITET

Abstract
The main focus of this thesis is the theoretical investigations of a nanogap platform used for molecular electronics measurements under ambient conditions. The nanogap is about 20 nm wide, while the molecules investigated here (octanethiol(OT) and octanedithiol(ODT)) are about 1-1.5 nm long making it impossible to bridge the gap with one molecule. Two different approaches are investigated. In the first approach the electrodes of the nanogap are coated with a layer of OT molecules, and large gold nanoparticles (diameter of about 30 nm) are trapped in the gap creating two molecular junctions with assemblies of molecules. In the second approach the electrodes are kept clean, but instead the gold nanoparticles are coated with doubly functionalized molecules (ODT) and trapped in the gap. Here the nanoparticles are limited in size to about 5 nm, hence it is necessary to consider nanoparticle-molecule chains or small networks to bridge the gap. The first principles modeling of the structure of the metal-molecule junctions combined with elastic and inelastic transport properties is performed using the density functional theory (DFT) combined with the non-equilibrium Green's functions (DFT-NEGF) method.

In the first approach with the coated electrodes and the large nanoparticles, simulations show that structural irregularities at the electrode interface can lead to a significant variation of the conductance through the molecular film. Due to the size of the nanoparticles, the shape and orientation of the facets will have great influence on how many molecules are connected, affecting the measured resistance of the device.

With the second approach utilizing the functionalized nanoparticles, more stable junctions are obtained since the nanogap is bridged by molecular junctions chemisorbed in both ends. To make chemical bonds to both sides of the junctions, the outer functional group needs to be protected before the trapping of nanoparticles in the gap. Deprotected nanoparticles agglomerate and cannot be trapped. We have investigated the most probable configurations of the molecules in these junctions. During deprotection of the functional group in the gap, a conduction increase have been observed. We have found that the removal of the protection group is not responsible for the increased conduction. Instead, since the deprotected molecule is shorter and the nanoparticles are mobile during deprotection, a reorganization of the nanoparticles in the gap occurs. This reorganization leads to decreasing of the tunneling length for the electrons, hence increasing the conduction.

We also demonstrate, that we can obtain the inelastic electron tunneling spectroscopy (IETS) signature of an octanedithiol molecule in this platform. This is done on the network of chemisorbed ODT junctions, where we are able to relate the low-bias Au-S and C-S stretch modes of the molecule to observed peaks in IETS. From this we estimate that the main contribution in the signal comes from chains containing 5, 6 and 7 molecular junctions. To identify the peaks, we have calculated the theoretical spectra for one molecule, from which we are able to extract the important vibrational modes, and their couplings to the electrons. This we then use in a model, including the Coulomb blockade observed in the nanoparticles, to fit the theoretical spectra to the measured one.

List of papers

This thesis is based on the following papers, which are referred to in the text by their Roman numerals.

I S. H. M. Jafri, T. Blom, K. Leifer, M. Strømme, H. Löfås, A. Grigoriev, R. Ahuja and K. Welch:
Assessment of a nanoparticle bridge platform for molecular electronics measurements
Nanotechnology 21, 435204 (2010)

II S. H. M. Jafri, H. Löfås, T. Blom, A. Wallner, A. Grigoriev, R. Ahuja, H. Ottosson and K. Leifer:
Realization of highly reproducible molecular junctions in a nanoparticle-alkanedithiol-nanoelectrode bridge platform
Manuscript

III K. Leifer, S. H. M. Jafri, H. Löfås, J. Agustsson, T. Blom, A. Grigoriev, J. Fransson, R. Ahuja, A. Wallner, M. Calame, and H. Ottosson:
Vibrational signatures in inelastic electron tunneling spectroscopy from short molecule-nanoparticle chains trapped in versatile nanoelectrodes
Manuscript

Reprints were made with permission from the publishers.

Papers not included in the Thesis

- H. Löfås, A. Grigoriev, J. Isberg and R. Ahuja:
Effective masses and electronic structure of diamond including electron correlation effects in first principles calculations using the GW-approximation
AIP Advances 1, 032139 (2011)
- B. Pathak, H. Löfås, J. Prasongkit, A. Grigoriev, R. H, Scheicher and R. Ahuja:
Double-functionalized nanopore-embedded gold electrodes for rapid DNA sequencing
Accepted Appl. Phys. Lett.

Contents

1 Introduction 7
1.1 Why molecular electronics? 7
1.2 Interfacing molecules 8
1.3 Outline 8

2 Theoretical framework 9
2.1 The many body problem 9
2.1.1 Born-Oppenheimer approximation 9
2.2 Density functional theory 10
2.2.1 Exchange-correlation functionals 11
2.3 Computational methods 12
2.3.1 Pseudopotentials 12
2.3.2 Basis set 13
2.4 Nuclear vibrations 13
2.5 Quantum transport in the non-equilibrium Green's functions formalism (NEGF) 14
2.5.1 System setup 14
2.5.2 Elastic Transport 15
2.5.3 Inelastic transport due to electron-phonon interaction 15
2.6 DFT as a framework for quantum transport 17

3 Nanoparticle bridge platform 18
3.1 Structural defects in molecule coated electrodes 18
3.2 Realization of highly reproducible molecular junctions in a nanoparticle-alkanedithiol-nanoelectrode bridge platform 21
3.3 Vibrational signatures in inelastic electron tunneling spectroscopy from short molecule-nanoparticle chains trapped in versatile nanoelectrodes 25

4 Conclusions and outlook 28

5 Acknowledgement 29

References 30

1. Introduction

Nanotechnology has developed to one of the fastest growing fields in today's science. A nanometer (nm) is one thousand millionth of a meter, which can be compared with a red blood cell which is 7000 nm wide or a water molecule that is of the order 0.3 nm. Nanoscience is the study of phenomena and manipulation that occur on the atomic or molecular scale (from 0.1 nm up to 100 nm) where often the properties differ significantly compared to those on the macro scale. This is often due to at the nanoscale quantum effects can be dominating, changing the optical, electrical and magnetic behavior drastically.

During the last decade the electronic devices have undergone a rapid development towards faster and smaller, the feature sizes have been reduced greatly and have reached the nanometer scale. The base of the integrated circuit is the silicon based complementary metal-oxide-semiconductor (CMOS), with feature sizes as small as 32 nm (soon to be 22 nm)[1]. The shrinking of the devices so far have followed what is called the Moore's law which states that the transistor density on integrated chips will double every two years[2]. This prediction was made in 1965[3] and has shown to be peculiarly correct, probably in large part due to that it now is used in the semiconductor industry as a roadmap for research and development. The end of the law have been predicted several times but still it is valid, and for the last 30 years it has been predicted that Moore's law would last at least another decade. By now the estimate is that somewhere between 2015 and 2020 we will reach the end (at least with today's CMOS devices) of Moore's law when small enough feature sizes are reached that the nanoscale quantum effects will introduce tunneling in the transistor making it unrealiable[4]. To circumvent the difficulties in miniaturization of the CMOS some other ideas have been proposed, for example to replace some parts in the CMOS with molecules, or build complete electronic devices with molecules as the active elements. This have emerged into what is now known as molecular electronics.

1.1 Why molecular electronics?

The idea of molecular electronics[5] is to build electronic components where the active element is provided by single or assemblies of molecules that can act as switches, gate-operated transistors and wires. The first proposed device was a molecular rectifier by Aviram and Ratner in 1974, where they showed a structure that could function as a rectifier and explained the theory why it was resonable[6]. The interest in molecular structures for use in electronic devices is based on four major advantages over silicon based devices.

- Size. Molecular structures are in the range between 1 and 100 nm. Smaller comes with lower cost (identical molecules can easily be produced in huge numbers), higher efficiency (only few electrons needed to transport a signal) and lower power dissipation (ultra-dense devices possible with molecules as active elements).
- Assembly and recognition. Molecules self-assemble to form regular structures which can be used to build devices. Molecular recognition can be used to modify electronic behavior on the single-molecule scale creating both molecular switches and sensors.
- Dynamical stereochemistry. Many molecules have multiple stable structures or isomers, which can have distinct different electronic and optical properties possible to use for switching devices.
- Synthetic tailorability. Chemical synthesis is a highly developed field where it is possible to engineer organic molecules with specific electronic properties changing the transport or optical properties of the molecule.

There are drawbacks also including instability at higher temperatures, noise due to low current density and slow switching speeds due to low transmission probabilities through contacts. But overall the advantages could break the way for molecules as active elements in future electronic applications.

1.2 Interfacing molecules

Molecular electronics is a rapidly emerging field, but still there are many great challenges that have to be overcome, even though proof-of-principle devices such as diodes and memories already have been demonstrated[6, 7, 8, 9, 10]. The interface between the electrodes and the molecules is one of the most important components of the molecular junction; it both can limit the current and also modify the measured response from the molecule due to changes in the intrinsic states in the molecule induced from the metal. One of the main challenges still today is to understand the coupling between the molecule and the macroscopic contacts, especially when they are under non equilibrium conditions such as when there is an external voltage applied to them. However, starting from the early work by Reed et al.[11], where they were able to measure the conductance (G) of benzene-1,4-dithiol (BDT) molecules in a mechanically controllable break junction (MCBJ) experiment, several experimental techniques have been developed for this task including scanning tunneling microscopy (STM), conducting probe atomic force microscopy (CP AFM), STM break junctions, a review of these and several other testbeds have been done by Akkerman and de Boer [12]. The reproducibility is still a big concern for the experimental measurements, but now it is customary of study the statics for formation of molecular junctions. Still there is a variety of reported values for the conduction of different molecules. Several theoretical studies[13, 14, 15, 16, 17, 18, 19] have also been done where the conductance varies several orders of magnitude for the same molecule depending on method and attachment.

1.3 Outline

The main focus of this thesis is the theoretical investigation of electron transport in a nanogap platform[20] which uses metallic nanoparticles for characterization of different molecular systems under ambient conditions. This includes first principles modeling of the structure and interface in the metal-molecule junctions combined with elastic and inelastic transport properties for a metal-molecule-metal device.

In **Chapter 2** the theoretical framework used here is introduced. The starting point is the Schrödinger equation of interacting particles which is then used to calculate the electronic structure for our system. This is done in the framework of density functional theory (DFT), and a basic description of the theory is given in the chapter. Further the method for electronic transport is introduced based on non equilibrium Green's function (NEGF) formalism. The expressions for both the elastic and inelastic conductance are discussed.

In the following chapter, **Chapter 3**, a summary of the obtained results when we apply the presented methods to describe measurements on a nanoparticle bridge platform will be given. We show that structural defects on the electrodes can significantly change the measured conductance. Further we investigate conformational changes in the junction during deprotection of doubly thiolated alkane chains and the protection groups influence on the conduction. In the last section we model the inelastic response of a network with molecule coated nanoparticles bridging the nanogap to get a better understanding of configurations and structure of the network.

At last in **Chapter 4** conclusions from our work and a outlook are presented.

2. Theoretical framework

In this chapter a brief overview of the theoretical framework used in this thesis is given. This work is based on density functional theory (DFT). The electronic structure of an atomic system is described from first principles (ab initio), or without parameters derived from experiments. In the first part of this chapter an overview of the main theorems starting from the many-body problem will be given.

In the following section a brief overview of some important aspects of implementation of DFT for the atomic-scale simulations is given, as employed for the electronic structure calculations in this thesis.

In the last part of the chapter, theory describing electron transport through a scattering region is introduced. This is based on nonequilibrium Green's functions (NEGF) theory and the description for both the elastic and inelastic current is introduced.

2.1 The many body problem

To describe a material we need to understand how a great number of atoms interact with each other, hence we are dealing with a many body problem. The properties we are interested in can be determined from the Schrödinger equation

$$\hat{H}\Psi = E\Psi \tag{2.1}$$

where the Hamiltonian, $\hat{H}$, describing the system is

$$\begin{aligned} \hat{H} &= -\frac{\hbar^2}{2}\sum_{k}^{N_{nucl}}\frac{\nabla^2}{M_k} - \frac{\hbar^2}{2}\sum_{i}^{N_{el}}\frac{\nabla^2}{m_e} \\ &+ \frac{1}{2}\sum_{k\neq l}^{N_{nucl}}\frac{Z_k Z_l e^2}{|\mathbf{R}_k - \mathbf{R}_l|} + \frac{1}{2}\sum_{i\neq j}^{N_{el}}\frac{e^2}{|\mathbf{r}_i - \mathbf{r}_j|} - \sum_{i,k}^{N_{el},N_{nucl}}\frac{Z_k e^2}{|\mathbf{r}_i - \mathbf{R}_k|} \end{aligned} \tag{2.2}$$

where the first two terms are the kinetic operators for the nuclei and electrons. The three terms on the second row describes the interaction between nuclei-nuclei, electron-electron and nuclei-electron respectively. This problem is extremely difficult to solve, and can only be solved exact in the simplest case, the hydrogen atom. For more complicated systems such as solids where a large number of particles are considered, approximations have to be done.

2.1.1 Born-Oppenheimer approximation

The first approximation done to solve the problem is the Born-Oppenheimer (BO)-approximation [22], where the motion of the electrons are separated from the nuclei. This can be done since the mass of the nuclei is much greater compared with the mass of the electrons, hence the nuclei can be considered static at its equilibrium position and interact with the electrons via an external potential, V_{ext}. The electronic Hamiltonian can now be written as

$$\hat{H} = -\frac{\hbar^2}{2}\sum_{i}^{N_{el}}\frac{\nabla^2}{m_e} + \frac{1}{2}\sum_{i\neq j}^{N_{el}}\frac{e^2}{|\mathbf{r}_i - \mathbf{r}_j|} + \hat{V}_{ext} \tag{2.3}$$

In the potential $\hat{V}_{ext}$ can other external effects such as electromagnetic fields also be included. Even if the Hamiltonian is simplified now, the electron-electron interaction is still there which makes the problem still complicated to solve. One approach to handle this is with DFT which will be considered in following section.

2.2 Density functional theory

The basic idea of DFT is to replace the more complicated many-body problem described in Eq. 2.2 and Eq. 2.3 with another system more easily solved. Still DFT is an exact theory, but in practice since the exact functional describing the interactions between electrons in the system is not known, some approximations to the Hamiltonian have to be done. The main foundation of DFT are the Hohenberg-Kohn theorems [23, 24], that states

Theorem 2.2.1 *If two systems of electrons have the same ground state density $\rho(\mathbf{r})$ while one is trapped in the potential $V(\mathbf{r})$ and the other in potential $V'(\mathbf{r})$ then,*

$$V'(\mathbf{r}) - V(\mathbf{r}) \equiv \text{const} \tag{2.4}$$

This implies since $V(\mathbf{r})$ is a unique functional of $\rho(\mathbf{r})$ (up to a constant), and $V(\mathbf{r})$ fixes H (Eq. 2.3), the many-particle ground state is a unique functional of the density $\rho(\mathbf{r})$.

Since the wave-function Ψ is a functional of the density, $\rho(\mathbf{r})$, it is possible to define a universal functional $F[\rho]$ valid for any number of particles and any external potential. With this functional it is possible to define the energy functional for the system as

$$E[\rho(\mathbf{r})] \equiv \int V(\mathbf{r})\rho(\mathbf{r})d\mathbf{r} + F[\rho(\mathbf{r})] \tag{2.5}$$

and show that

Theorem 2.2.2 *The global minimum of the energy functional (Eq. 2.5) is the true ground-state energy, E_0, for the system and the density that minimize the functional is the ground-state density, $\rho_0(\mathbf{r})$*

This implies that if we would know $F[\rho]$ and it was sufficiently simple functional of ρ it would be an easy task to determine the ground-state density and energy of the system for a given external potential. However for the majorities of problems the universal functional is not known and have to be approximated in some way. Still the two theorems shows the strength of DFT, mapping the many-body problem to the electron density.

To further simplify the problem a first approximation were proposed by Kohn and Sham [24] where they assumed that instead of the interacting electrons we have a system of non-interacting electrons moving in a effective potential. Thus, reducing the many-body problem to a single-particle problem of electrons described by the Kohn-Sham eqution,

$$H\Phi_j(\mathbf{r}) = \epsilon_j\Phi_j(\mathbf{r}) \tag{2.6}$$

with $\Phi_j(\mathbf{r})$ as the Kohn-Sham (KS)-wavefunction with eigenvalue ϵ_j and where the Hamiltonian for the system is

$$H = -\frac{\nabla_i^2}{2} + V_{\text{eff}}(\mathbf{r}) \tag{2.7}$$

and

$$V_{\text{eff}}(\mathbf{r}) = V_{\text{ext}} + \int \frac{\rho(\mathbf{r}')}{|\mathbf{r} - \mathbf{r}'|}d\mathbf{r} + \frac{\delta E_{xc}[\rho(\mathbf{r})]}{\delta\rho(\mathbf{r})}. \tag{2.8}$$

The effective potential is described by three terms, first the external potential that includes the interaction between the ion cores and the valence electrons, the second term is the Coulomb potential. The third term, the exchange-correlation functional, is the most complicated and can not up to today be evaluated exactly but have to be approximated in some way.
The Kohn-Sham wavefunctions in Eq. 2.6 are not the true wavefunctions for the system, but they can be used to calculate the electron density as

$$\rho(\mathbf{r}) = \sum |\Phi_i(\mathbf{r})|^2 \tag{2.9}$$

To obtain the ground-state density, the Kohn-Sham equations can be solved iterative until self-consistency (difference between input and output density less than some convergence criteria) is reached as follows

1. Make an initial guess of the electron density $\rho(\mathbf{r})$.
2. Construct the effective potential from Eq. 2.8
3. Solve Eq. 2.6 to obtain the KS-wavefunctions $\Phi_j(\mathbf{r})$
4. Calculate the density according to 2.9
5. Compare the input density and the new density obtained in the previous step, if the difference is less than the convergence criteria the problem of finding the ground-state density is solved. Otherwise use the new density as input to step 1 and iterate until convergence.

2.2.1 Exchange-correlation functionals

To be able to solve the Kohn-Sham equations in the previous section, we have to specify some expression for the exchange-correlation functional $E[\rho(\mathbf{r})]$, but since the exact form of this functional is unknown it is necessary to find a approximative form. In the orginal work of Kohn and Sham [24] they introduced an expression for the functional which have later been called the local density approximation (LDA).

$$E_{xc}[\rho] = \int \rho(\mathbf{r})\epsilon_{xc}(\rho(\mathbf{r}))d\mathbf{r}, \tag{2.10}$$

where $\epsilon_{xc}(\rho)$ is the exchange-correlation energy per electron of a uniform electron gas of density $\rho(\mathbf{r})$, which is known from the theories of the homogenous electron gas. It can be shown that this functional is more or less exact in two limiting cases,

(a) Slowly varying density In this limit the condition $r_s/r_0 \ll 1$ holds, where r_s is the Wigner-Seitz radius and r_0 is the length scale of the density variation. It is possible to show that the above expression (2.10) is then exact if terms of $|\nabla|^2$ and higher order in the energy is neglected, giving the density with even higher accuracy with errors of the order $|\nabla|^4$.

(b) High density This limit is characterized by the condition $r_s/a_0 \ll 1$, where a_0 is the Bohr radius. This implies that energy from exchange and correlation effects is significantly smaller (by a factor of r_s/a_0) than the kinetic energy of the electrons, hence the inaccuracy in the exchange-correlation energy is neglible.

Correspondingly atoms and molecules can be divided into three regions: First we have the region close to the atomic nuclei, where the electronic density will be high, hence LDA should be ok from (b). Secondly, far away from the nucleus the electronic density can be expected to vary slowly, and LDA is good according to (a). Third and last we have the intersitial region between atoms in molecules and solids. Here LDA can not be expected to work and this should be the main source of errors in the calculations using LDA, hence the description of chemical bonding should not be accurate. Supringsly, LDA works very well for solids, even for solids with properties far from the homogenous electron gas, but in most cases the binding energy is overestimated[25].

There have been many attemps after the first LDA functional to come up with something better. Maybe the most well-known and used of these is the generalized gradient approximation (GGA), where the exchange-correlation energy per atom ϵ_{xc} is not just calclated from the density but also the gradient of the density, $\nabla\rho(\mathbf{r})$. There exist many forms of this functional, where probably the Perdew-Wang (PW92)[26] and Perdew-Burke-Ernzerhof (PBE)[27] are the most used. There is no general results which of the functionals that are most accurate, instead they have to be evaluated from problem to problem and compared to experiments. Still it is known that GGA always gives a smaller exchange-correlation energy, hence decreasing the binding energy and correcting the LDA over-binding. This often improves the agreement with experiments, but can also lead to under-binding.

In this thesis, LDA (and GGA to double check the results) will be used, and when investigating transport the choice between the functionals should not be as important as dealing with the structure, since the difference between the functionals will be small compared to approximations in the transport calculations.

2.3 Computational methods

To use DFT for numerical calculations many technical details and further approximations have to be done. In this work the SIESTA (Spanish Initiative for Electronic Simulations with Thousands of Atoms) code will be used, some of the main aspects of the implementation are briefly described below, a full description of the code is available in Refs. [21, 28] and references therein.

2.3.1 Pseudopotentials

To make the atoms more computationally cheap it is possible to replace the effect of the the motion of the core electrons of an atom and its nucleus with some effective potential. The pseudopotential is an effective potential used to describe the chemically inert core, while the valence states active in chemical bonding are treated explicity[29]. This is possible to do since the core-electron wave function of an atom stays almost unchanged in different chemical enviroments, and the major role of the core-electron wave functions in chemical bonding is to constrain the valence states to be orthogonal to the core states. With just this constrain the possibilities to generate a pseudopotential are infinite, therefore there have been a lot of work of finding a way to generate sutiable pseudopotentials that both reproduces the all-electron behaviour and in the same time are computationally efficient.

The pseudopotentials used in the calculations are generated from all-electron atomic calculations, this is done in DFT by solving the radial Kohn-Sham equation[24]

$$\left(\frac{-1}{2}\frac{d^2}{dr^2} + \frac{l(l+1)}{2r^2} + V[\rho;r]\right) rR_{nl}(r) = \epsilon_{nl} R_{nl}(r) \tag{2.11}$$

where $V[\rho;r]$ is the self-consistent one-electron potential

$$V[\rho;r] = \frac{-Z}{r} + V_H[\rho;r] + V_{xc}^{func}(\rho(r)), \tag{2.12}$$

$\rho(r)$ is the sum of electron densities for the occupied wavefunctions $R_{nl}(r)$, $V_H[\rho;r]$ is the Hartree potential and $V_{xc}^{func}(\rho(r)$ is the exchange-correlation potential for the used functional (func=GGA,LDA). Further the pseudopotentials are constructed to satisfy four general conditions.

- The pseudo-wave-functions generated from the pseudopotential should contain no nodes.
- The normalized atomic radial pseudo-wave-function (PP) with angular momentum l is equal to the normalized radial all-electron wave-function (AE) beyond a chosen cutoff radius r_{cl},
$$R_l^{PP}(r) = R_l^{AE}(r) \qquad \text{for} \qquad r > r_{rcl}. \tag{2.13}$$
- The charge inside the cutoff-radius must be the same for the two wave-functions (PP and AE)
$$\int_0^{r_{cl}} |R_l^{PP}(r)|^2 r^2 dr = \int_0^{r_{cl}} |R_l^{AE}(r)|^2 r^2 dr. \tag{2.14}$$
- The last criterion is that the AE and PP eigenvalues should be equal
$$\epsilon_l^{PP} = \epsilon_l^{AE}. \tag{2.15}$$

The pseudopotentials constructed and fulfilling these criterias are usually referred to as "norm-conserving pseudopotentials"[30] and it is this type that is commonly used in SIESTA calculations. These psuedopotentials can be constructed in several ways, in SIESTA usually the parametrization by Troullier and Martin[29] is used where the semilocal form of the pseudopotential is transformed to the fully nonlocal form by the method av Kleinman and Bylander[31].

2.3.2 Basis set

In the SIESTA method the valence electrons are described by a basis set consisting of linear combination of localized numerical atomic orbitals (LCAO). That means that the basis are composed of a spherical harmonic and a radial function

$$\Phi_{lmn}(r,\theta,\varphi) = R_{n,l}(r)Y_{l,m}(\theta,\varphi) \tag{2.16}$$

where $R_{n,l}$ and $Y_{l,m}$ are the radial function for orbital n and real spherical harmonic for orbital angular momentum l and magnetic quantum number m. The use of a localized basis set have an advantage of the more commonly used plane-wave basis sets especially when dealing with transport in open quantum systems due to the finite radius, r_c, of the basis orbitals, making them strictly zero beyond this radius. Further the shape and size of the basis set must be chosen, where there are a lot of freedom how to build them. This include the center (not necessarily atom centered), how many angular momentum channels around each center, how many radial functions per angular momentum channel and last the cut-off, r_c, and shape for each radial function. These parameters should be chosen wisely to optimize the struggle between efficiency and accuracy. There are methods to obtain optimized basis sets variationally[32] but still there is no systematic way to obtain "the optimal" basis set and check the convergence. Still SIESTA comes with some preset algorithms and criteria defining basis sets automatically[33].
In SIESTA the nomenclature of the basis sets follows the quantum chemistry (QC) standards, ranging from basis sets of single ζ (SZ) type to multiple ζ including polarization and diffuse orbitals, giving results from fast calculations with poor convergence to highly converged and more computationally demanding calculations. The minimal basis set is the SZ which has one radial function per angular momentum channel, the number of angular functions are determined by electronic population of the valence states in the free atom. To obtain flexibility in the radial part, it is possible to add one more radial function a get a double-ζ (DZ) basis. In SIESTA this is done in a similar fashion as the split-valence scheme in QC but with a modification to make sure that the finite range of the basis is kept[34], where the new radial function are equal to the first one outside a matching radius, only changing the part closes to the core. In this fashion it is also easy to extend to even more radial functions and get a multiple-ζ basis. To introduce more flexibility in the angular part, polarization orbitals can be added. The first choice for this would be to use the first unoccupied orbital of the free atom, but it has been found that this is not a good choice since they are generally to extended. Instead another route have been found where a small electric field is used to polarize the atom resulting in in the (l+1) orbital.

The methods described here has been thoroughly tested and the results have shown that for structural and energetical properties most often a DZ plus one polarization orbital (DZP) basis set gives results within the accuracy of the LDA and GGA approximation.

2.4 Nuclear vibrations

If we now have solved Eq. 2.1 within the BO-approximation we know the energy-eigenvalues for our system and have something called the Born-Oppenheimer total energy surface $E(\mathbf{R})$. From this it is possible to investigate the vibrational modes in the system, i.e phonons[35], via the forces. If the system is in the equilibrium geometry ($\mathbf{R}_0$) all forces on the nuclei should be zero

$$\mathbf{F}(\mathbf{R}_0) = -\left.\frac{\partial E_0(\mathbf{R})}{\partial \mathbf{R}_I}\right|_{\mathbf{R}=\mathbf{R}_0} = 0 \tag{2.17}$$

If a small perturbation is introduced as a displacement away from the equilibrium geometry the matrix of interatomic force constants called the Hessian matrix is obtained

$$C_{I\nu;J\mu} \equiv \left.\frac{\partial^2 E_0(\mathbf{R})}{\partial R_{I\nu}\partial R_{J\mu}}\right|_{\mathbf{R}=\mathbf{R}_0} \tag{2.18}$$

where μ,ν represents the different spatial directions. Assuming a harmonic displacement of the coordinates and using Newtons's second law of motion the eigenvalue problem

$$(\omega^2\mathbf{1} - \mathbf{W})\mathbf{v} = 0 \tag{2.19}$$

is obtained where $\mathbf{W}$ is the mass-scaled matrix of interatomic force constants

$$W_{I\nu;J\mu} \equiv \frac{C_{\nu;J\mu}}{\sqrt{M_I M_J}} \tag{2.20}$$

The solution of Eq. 2.19 gives the vibrational frequency ω_λ and vibrational mode vector $\mathbf{v}^\lambda$ for our system.
The nuclear forces $\mathbf{F}_I$ are readily available during the solution of the DFT-problem and when the SIESTA package is used they are a direct output. These can then be used to approximate the Hessian matrix via finite differences in what is called the "frozen phonons method", more on how this can be done and the implications can be found in [21, 36].

2.5 Quantum transport in the non-equilibrium Green's functions formalism (NEGF)

In this section the basic equations describing the stationary electron transport through a region in space in NEGF formalism is given

So far in the previous sections we dealt with the DFT-method for electronic structure, the strength of DFT is that it from first-principles can describe a wide range of materials without some material-dependent parameters. Still, if we want to consider the electron transport we need to go beyond DFT due to its restrictions, first; it can only treat small finite or periodic systems and second; the system has to be in its equilibrium ground state. Here, when a atomic or molecular system is connected to bulk electrodes we need to be able to treat infinite and non-periodic systems. Further, to drive a current through this system, a bias voltage needs to be added to the electrodes, hence the molecular system will no longer be in thermal equilibrium and we must be able to treat this non-equilibrium system.

The starting point when using the NEGF approach is partition of the system into a central coupling region (which can include interactions) and two noninteracting electrodes, a sketch of the system is given in Fig. 2.1. In the following we assume that the system as in the case of DFT can be described by a single-particle mean-field Hamiltonian describing electrons moving in a static potential from the frozen atomic nuclei. For simplicity, the presentation will be given for spin-independent problems, but the generalization to include spin-polarization is straightforward.

2.5.1 System setup

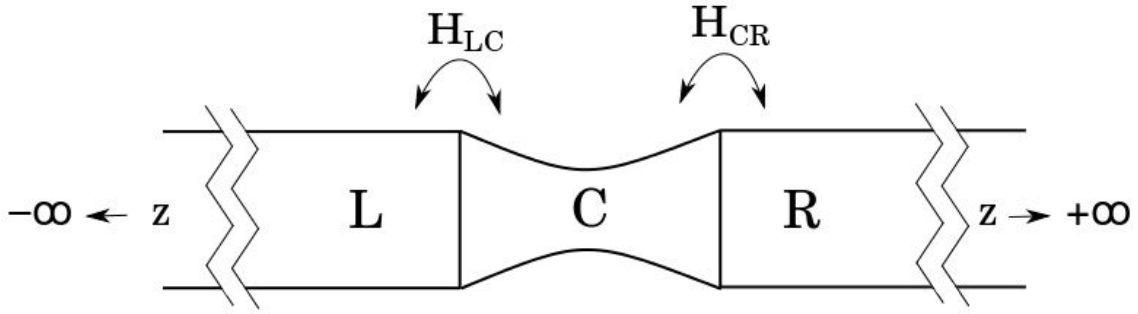

Figure 2.1: We model the contact C region coupled to two semi-infinite left L and right R electrodes. The direction of transport is denoted by z. There is no direct coupling between the two electrodes

The physical system we are interested in is sketched in Fig. 2.1, consisting of two semi-infinite electrodes coupled via a contact region. Since we are working in a framework of a localized basis set, the finite range of the orbitals implies that all matrix elements of the Hamiltonian or overlap integrals between atoms situated on the two different electrodes are zero, hence the only coupling between the left and the right electrode is via the contact region (provided that the contact region is large enough). The electronic Hamiltonian $\mathbf{H} \equiv \{\{H_{ij}\}\}$ and overlap matrix $\mathbf{S} \equiv \{\{S_{ij}\}\}$ can

thus be written as

$$\mathbf{H} = \begin{pmatrix} \mathbf{H}_L & \mathbf{H}_{LC} & 0 \\ \mathbf{H}_{CL} & \mathbf{H}_C & \mathbf{H}_{CR} \\ 0 & \mathbf{H}_{RC} & \mathbf{H}_R \end{pmatrix} \tag{2.21}$$

$$\mathbf{S} = \begin{pmatrix} \mathbf{S}_L & \mathbf{S}_{LC} & 0 \\ \mathbf{S}_{CL} & \mathbf{S}_C & \mathbf{S}_{CR} \\ 0 & \mathbf{S}_{RC} & \mathbf{S}_R \end{pmatrix} \tag{2.22}$$

The assumption is further that the Hamiltonian is converged to the bulk values in the L- and R-regions corresponding to the left and right electrodes. Thus it is only necessary to calculate the Hamiltonian and overlap matrices in the C, C-L and C-R regions.
The transport properties can thus be described by the finite L-C-R region of the infinite system, via a series of Green's function matrices. The retarded electronic single-particle Green's function $\mathbf{G}^r(\epsilon)$ describing the infinite system can be defined as the inverse of $[(\epsilon + i\eta)\mathbf{S} - \mathbf{H}]$ where $\eta = 0^+$[37]. For the contact region (C) this will then yield the retarded Green's function

$$\mathbf{G}^r_C(\epsilon) = [(\epsilon + i\eta)\mathbf{S}_C - \mathbf{H}_C - \mathbf{\Sigma}^r_L(\epsilon) - \mathbf{\Sigma}^r_R(\epsilon)]^{-1} \tag{2.23}$$

where the self-energy due to the coupling to the left lead is $\mathbf{\Sigma}^r_L(\epsilon) = (\mathbf{H}_{CL} - \epsilon\mathbf{S}_{CL})\mathbf{g}^r_L(\epsilon)(\mathbf{H}_{LC} - \epsilon\mathbf{S}_{LC})$ and similarly for the right lead. The $\mathbf{g}^r_\alpha(\epsilon)$ is the retarded surface Green's function of the $\alpha = L, R$ lead.

2.5.2 Elastic Transport

In the following we will consider a two-terminal setup without interactions in the central region (C), for this situation the current through this region can be described by the Landauer-Büttiker formula[38]

$$\begin{aligned} I(V) = G_0 \int_{-\infty}^{\infty} d\epsilon \, [n_F(\epsilon - \mu_L) - n_F(\epsilon - \mu_R)] \\ \times \mathrm{Tr}\,[\mathbf{\Gamma}_L(\epsilon)\mathbf{G}^r_C\mathbf{\Gamma}_R(\epsilon)\mathbf{G}^a_C(\epsilon)] \end{aligned} \tag{2.24}$$

where $G_0 = 2e^2/h$, $n_F = 1([exp(\epsilon/k_BT) + 1]$ is the Fermi-Dirac distribution, μ_α the chemical potential of lead α, and

$$\mathbf{\Gamma}_\alpha(\epsilon) \equiv i\,[\mathbf{\Sigma}^r_\alpha(\epsilon) - \mathbf{\Sigma}^a_\alpha(\epsilon)] \tag{2.25}$$

describes the broadening of the states in the central region by the coupling to the electrodes. This expression can be derived from the dissipation-fluctuation theorem[38]. The expression for the current is not general but only valid for a mean-field theory like the KS-DFT, also since we are dealing with steady-state transport the advanced and retarded Green's function can be related via time-reversal symmetry as $\mathbf{G}^a_C(\epsilon) = \mathbf{G}^r_C(\epsilon)^\dagger$. Further from Eq. (2.24) the expression for the transmission T can be identified.

$$T = \mathrm{Tr}\,[\mathbf{\Gamma}_L(\epsilon)\mathbf{G}^r_C\mathbf{\Gamma}_R(\epsilon)\mathbf{G}^a_C(\epsilon)] \tag{2.26}$$

2.5.3 Inelastic transport due to electron-phonon interaction

To investigate inelastic effects in the junction, excitations of phonons have to be taken in account. This can be done by the mass scaled dynamic matrix $\mathbf{W}$ (Eq. 2.20), and since interatomic forces are short ranged, it can be partitioned in the same way as $\mathbf{H}$ and $\mathbf{S}$.

$$\mathbf{W} = \begin{pmatrix} \mathbf{W}_L & \mathbf{W}_{LC} & 0 \\ \mathbf{W}_{CL} & \mathbf{W}_C & \mathbf{W}_{CR} \\ 0 & \mathbf{W}_{RC} & \mathbf{W}_R \end{pmatrix} \tag{2.27}$$

In the same way as we defined the electronic Green's function (Eq. 2.23) earlier, we can now define the retarded phonon Green's function $\mathbf{D}^r(\omega)$ as the inverse of $[(\omega + i\eta)^2\mathbf{1} - \mathbf{W}]$, for the contact region this gives

$$\mathbf{D}^r_C(\omega) = [(\omega + i\eta)^2\mathbf{1} - \mathbf{W}_C - \Pi^r_L(\omega) - \Pi^r_R(\omega)]^{-1} \tag{2.28}$$

where $\Pi^r_{R(L)}(\omega)$ are the phonon self-energies due to the coupling to right (left) regions. Since we are only interested in interactions between the electronic current and vibrations localized in the central region, to a first approximation, it is possible to disregard the phonon self-energies[36] resulting in

$$\mathbf{D}^r_C(\omega) \approx [(\omega + i\eta)^2\mathbf{1} - \mathbf{W}_C]^{-1} \tag{2.29}$$

Lowest order expansion of the current

To fully take into account the electron-phonon interactions when calculating the current is a very daunting task, where the full Green's functions $\mathbf{G}^{\gtrless}_C(\epsilon)$ including all relevant interactions are needed[36, 39, 40]. Even if this can be done, for systems with a weak electron-phonon coupling and where the density of states varies slowly with energy (which is the cases considered in this thesis) another approximation can be done, what is called the lowest order expansion (LOE) of the current, for the applicability of LOE see [39, 41]

The assumptions of LOE is that the retarded(advanced) single-particle Green's functions $\mathbf{G}^{r(a)}_C$ and lead self-energies $\Sigma^{r(a)}_\alpha$ are energy independent. Thus expanding the current to second order in the electron-phonon couplings $\mathbf{M}^\lambda$[36], the energy integrals can be done analytically, still preserving the Pauli exclusion principle for fermonic particles necessary for blocking of phonon emission processes at low bias.

The current in LOE approximation can be written as[36, 42]

$$\begin{aligned} I^{LOE} &= G_0 V \mathrm{Tr}[\mathbf{G}\mathbf{\Gamma}_R\mathbf{G}^\dagger\mathbf{\Gamma}_L] \\ &\quad + \sum_\lambda \mathcal{I}^{sym}_\lambda(V,T,\langle n_\lambda\rangle)\mathrm{Tr}\left[\mathbf{G}^\dagger\mathbf{\Gamma}_L\mathbf{G}\left(\mathbf{M}^\lambda\mathbf{A}_R\mathbf{M}^\lambda + \frac{i}{2}(\mathbf{\Gamma}_R\mathbf{G}^\dagger\mathbf{M}^\lambda\mathbf{A}\mathbf{M}^\lambda - H.C)\right)\right] \\ &\quad + \sum_\lambda \mathcal{I}^{asym}_\lambda(V,T)\mathrm{Tr}\left[\mathbf{G}^\dagger\mathbf{\Gamma}_L\mathbf{G}\left(\mathbf{\Gamma}_R\mathbf{G}^\dagger\mathbf{M}^\lambda(\mathbf{A}_R - \mathbf{A}_L)\mathbf{M}^\lambda + H.C\right)\right], \end{aligned} \tag{2.30}$$

$$\mathcal{I}^{sym}_\lambda = \frac{e}{\pi\hbar}\left(2eV\langle n_\lambda\rangle + \frac{\hbar\omega_\lambda - eV}{e^{(\hbar\omega_\lambda - eV)/k_BT} - 1} - \frac{\hbar\omega_\lambda + eV}{e^{(\hbar\omega_\lambda + eV)/k_BT} - 1}\right), \tag{2.31}$$

$$\mathcal{I}^{asym}_\lambda = \frac{e}{\hbar}\int_{-\infty}^{\infty}\frac{d\epsilon}{2\pi}[n_F(\epsilon) - n_F(\epsilon - eV)]\mathcal{H}_{\epsilon'}\left(n_F(\epsilon' + \hbar\omega_\lambda) - n_F(\epsilon' - \hbar\omega_\lambda)\right)(\epsilon) \tag{2.32}$$

where $eV = \mu_R - \mu_L$ is the bias, $\mathcal{H}$ the Hilbert transform and $\langle n_\lambda\rangle$ the expectation value of the occupation of phonon mode λ. Here $\mathbf{G} = \mathbf{G}^r_C(\epsilon_F)$ is the retarded Green's function and $\mathbf{A} = i(\mathbf{G} - \mathbf{G}^\dagger)$ the spectral function, which together with the electrode couplings $\mathbf{\Gamma}_{L,R} = \mathbf{\Gamma}_{L,R}(\epsilon_F)$ all are evaluated at the Fermi energy.

The current in the LOE representation contains three main parts, first is the Landauer-Büttiker term (cf. Eq. 2.24) for elastic conductance, secondly there is a "symmetric" term that gives symmetric conductance steps at vibrational energies, third and last is the "asymmetric" term which gives peaks and dips in the conductance that are asymmetric with respect to voltage inversion. Often the asymmetric contribution is small compared to the symmetric, and for symmetric junctions it can be shown that the asymmetric contribution is strictly zero. The symmetric term is also responsible for the sign of the conductance change, and the thumb rule is that it gives a conduction increase for low conducting systems (and a decrease for high conducting systems), hence phonons help electrons tunnel through not so well conducting molecules and introduce scattering centers in metallic wires with close to ballistic conduction. A more deep discussion about these features can be found in [42, 43, 44]

2.6 DFT as a framework for quantum transport

The method of Kohn-Sham DFT, described in an earlier section, have turned out to be one of the most successful methods describing equilibrium properties of materials. This have also made it a natural choice as starting point for electron transport calculations. Combining the two, also turned out to be very successful when describing semi-infinite systems under non equilibrium conditions. As in the case of DFT where trends in the energy is reproduced very well, here trends in the electron transport between similar systems are reproduced very well. Making it possible to do quantitive estimations that can be compared to experiments and predictions that can be used as a guide for new experiments..

Still one needs to be cautious, since not only approximations related to DFT described earlier, but also some more maybe not as well-founded approximation where the Kohn-Sham (KS) wavefunctions are treated as the "real" single-particle wave functions when the current is calculated. This mean that we assume that the KS-wavefunctions describe the true electron wavefunctions well enough (which we know is not always the case) and that the commonly used XC-functionals can describe the non-equilibrium situation we are dealing with. Since we are only using the single-particle wavefunctions, this method will not describe many-body effects, which often are present at transport processes. It is widely known for example that commonly used DFT-methods and functionals underestimates the gap between the highest occupied molecular orbital (HOMO) and lowest unoccupied molecular orbital (LUMO), hence conductance of many molecules weakly coupled to the electrodes are overestimated, this can often be corrected if correlation effects are included for example via GW or self-interaction correction.[37, 45, 46, 47, 48]

As mentioned earlier, the convergence of the basis set is a delicate task, doing transport calculations it may turn out to be even harder to define what convergence is. There have been some tries to make a benchmark of basis sets for transport calculations [49]. The main conclusion is that as in the case of structural convergence in DFT a DZP-basis is often enough for transport, increasing more can give even a “better” result when they compare to plane-wave calculations. For just a qualitative result a SZ or SZP are enough since it reproduces the shape of the transmission function ok. It has also been found that the Fermi level and some molecular orbitals (MO) are very sensitive to the size of the basis set, changing the basis could shift the Fermi level in/out from the HOMO-LUMO gap or reorder MOs, hence changing the transmission by orders of magnitude[50, 51]. This could alter the interpretation of the conductance between for example different conformers of a molecule significantly. Using the same basis sets, functionals and other parameters when comparing similar systems should overcome most of these difficulties.

3. Nanoparticle bridge platform

In this work theoretical studies of a nanogap platform[20] are done, using metallic (gold) nanoparticles to bridge the gap between the electrodes and to characterize different molecular systems under ambient conditions. The system is advantageous since it is simple enough to test different molecular systems repeatedly with good statistics and it can be done under ambient conditions, i.e. it is possible to use it in an actual device. In a first setup, large enough (30nm) gold nano particles (AuNP) were chosen to bridge the nanogap by one single AuNP and contact the molecular film coated on both electrodes (Paper I). To get a better reproducibility and stability of the contacts, instead of coating the electrodes with molecules the AuNP were functionalized with molecules, opening the possibility for chemical bonding to the gold surface with both ends of the molecule (Paper II). The drawback of this setup was that it used smaller (5nm) AuNPs, hence a network of metal-molecule-metal contacts are needed to bridge the gap. To investigate different configurations of this network IETS measurements have been carried out (Paper III).

3.1 Structural defects in molecule coated electrodes

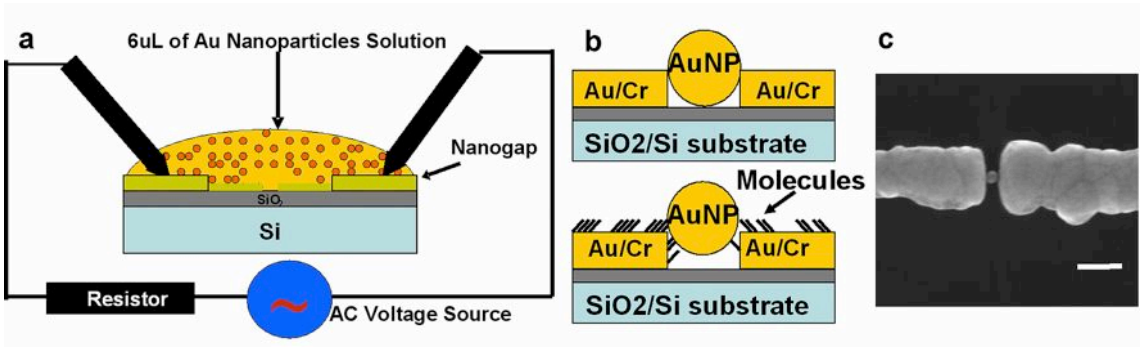

Figure 3.1: a) Schematic of the nanoelectrode setup during a trapping experiment in which probe needles were connected to the contact pads and 6 μL of an aqueous AuNP solution was deposited on top. b) Schematic cross section of a nanogap with one AuNP trapped between non-functionalized electrodes (upper image) and functionalized electrodes (lower image). c) Scanning electron microscope image of a single trapped AuNP in a nanogap. The scale bar is 100nm

Alkanethiol molecules often serve as a prototype model for studies of molecular electronic junctions. Previous studies using scanning probe microscopy techniques have considered both SAMs[17, 52] and unimolecular junctions[13] where the probe tip is modeled as an atomic wire or an atomic protrusion. Still there is a large uncertainty in the conductance of the octanethiol chain where the values varies by more than 1 order of magnitude ($G \sim 1 - 20 \times 10^{-5} G_0$, G_0 is the conductance quantum). The discrepancies are assigned to microscopically different junctions with for example different molecule-electrode bonding or different molecular conformations.

The setup considered in this section is shown in Fig. 3.1 where both a schematic of the trapping and final device are shown (a) and (b). A scanning electron microscope (SEM) image from one of the actual devices is also shown. A more detailed description of the platform and the trapping is given in [20] and Paper 1, here the focus will be on the theoretical calculations of the junctions. This setup shows even larger variations in the octanethiol conduction compared to previous stuides, as seen in Fig. 3.2, due to several reasons including no well-defined molecular conformations, several molecules in the junction and very rough gold surface due to the focused ion-beam (FIB) cutting of the gaps.

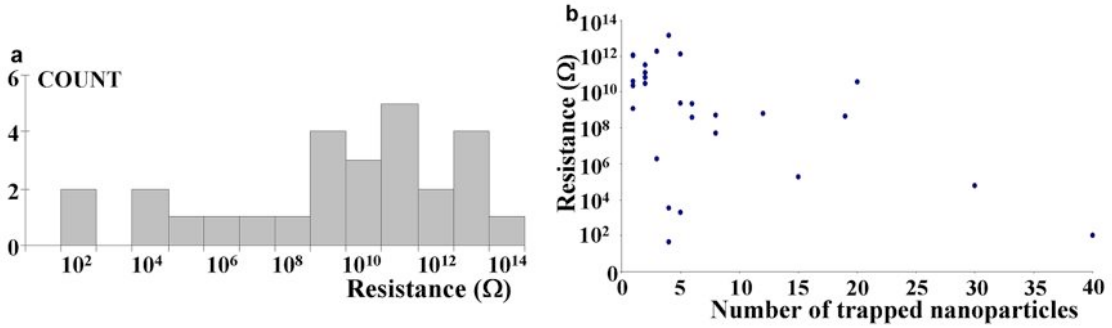

Figure 3.2: (a) Resistance histogram of trapped AuNPs between octanethiol coated nanoelectrodes. (b) Variation in measured resistance as a function of number of trapped AuNPs.

To model the roughness of the FIB cut electrodes under the film of molecules we used a gold surface of (110)-symmetry which had undergone reconstruction[53] creating facets with local (111)-symmetry.

We obtained bond lengths and density of states projected (PDOS) on the adsorbed molecules that compare well with previous results, where a flat Au(111):OT interface was considered[54] due to the local (111)-symmetry of our electrodes. The surface reconstruction is not lifted upon molecular film adsorption. The shortest inter-electrode distance (see table 3.1) was obtained by minimizing the energy of the simulation cell with respect to electrode separation in which the molecules are sandwiched in the junction; all atomic coordinates were additionally relaxed with the electrodes fixed at the chosen distance. For the electron transport calculations, we considered three different setups in which the opposing electrode surfaces are: (1) structurally symmetric but laterally displaced (moved, figure 3.3a), (2) reconstructed and flat (unreconstructed) (figures 3.3b and 3.3d), and (3) spatially symmetric (figure 3.3c). With our setup the Au surface is quite deeply corrugated, yet no artificial patterns were used to model the corrugation.

Table 3.1: *Results from DFT and electronic transport calculations*

System name (see figure 3.3)	a)	b)	c)	d)
Distance between electrodes (Å)[a]	7.76	8.43	8.87	10.29
Δ E (eV)[b]	0	2.20	1.10	8.31
Zero-bias transmission T ($G_0 \times 10^{-3}$)	12.3	4.5	0.65	0.3
Resistance/mol (MΩ)	2.1	5.7	39.7	86

[a] The distance between electrodes is the distance between two nearest Au-atoms from different electrodes.

[b] Δ E is the difference in total energy between the different contact configurations where system a) (moved) has the lowest energy.

To analyze how the effective thickness of the molecular film affects the resistance, we consider the results collected in table 1. It is apparent that only one of the two molecules shown in Fig. 3.3c, and especially in Fig. 3.3d, is properly connected to the topmost electrode surface. If we account for this difference, the transmission decay can be estimated as $e^{-\beta L}$,$\beta = -0.7$ Å^{-1}, where L is the shortest distance between the electrodes, or in other words the "efficient" length of the molecules. This observation demonstrates that, adsorbed at non-ideal surfaces, molecules experience a larger contact area with the electrode, which, coupled with the fact that they are tilted at an angle of $-52.5°$ [17] with respect to the surface normal, results in a decreased effective length between electrodes and increased inter-molecular tunneling. Thus, the effective resistance of the molecules is decreased. The obtained magnitude of the transmission decay correlates well with experimental values [15, 52]; however, the estimated resistances are far too low in comparison with measured ones, which is expected for the method used[15]. To further describe what we mean by the different effective lengths between the molecules we plot the current densities in Fig. 3.4. Assuming a small positive bias on the bottom electrode, the currents flowing up through the

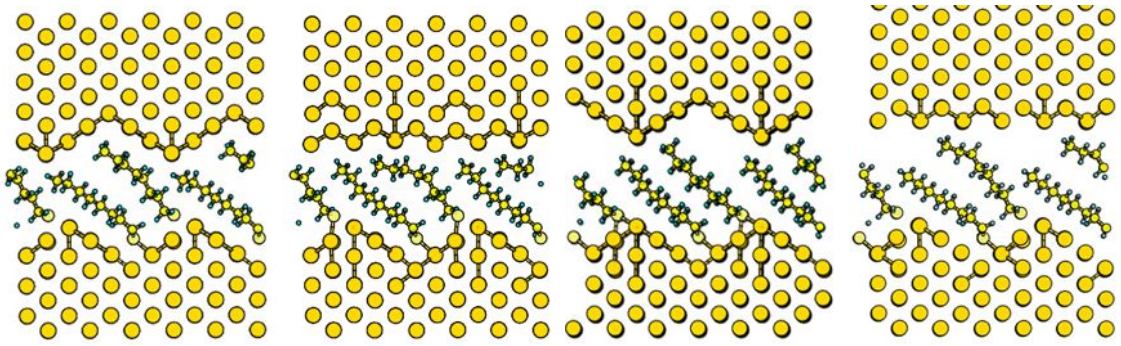

(a) "moved" *(b)* "flat" *(c)* "symmetric" *(d)* "flat+2Å"

Figure 3.3: Atomic configurations considered in theoretical simulation-side view of the contact area seen along the [$\bar{1}$10] direction. Different structures obtained by moving the top electrode correspond to different inter-electrode separations (see table 3.1). a) Symmetric but laterally displaced electrodes, b) reconstructed and flat surfaces, c) spatially symmetric surfaces and d) same as b), but additionally spaced by 2 Å.

molecule are plotted, where the cross-section of the arrows is proportional to the magnitude of the current density. We can see that setup (a) and (b) shows very similar behavior, where the current flows almost straight through the junction, either tunneling from the top gold atom or via the left anchoring sulphur atom straight to the top of the right molecule (intermolecular tunneling) and to the top gold electrode. Giving the effective length as the distance from the top gold atom on the bottom electrode to the bottom gold atom on the top electrode. In setup (c) instead we can see that the main current path is along the backbone of the left molecule, and the effective length has to measured along the molecule instead, increasing it greatly hence it has much lower transmission probability as seen in the table above.

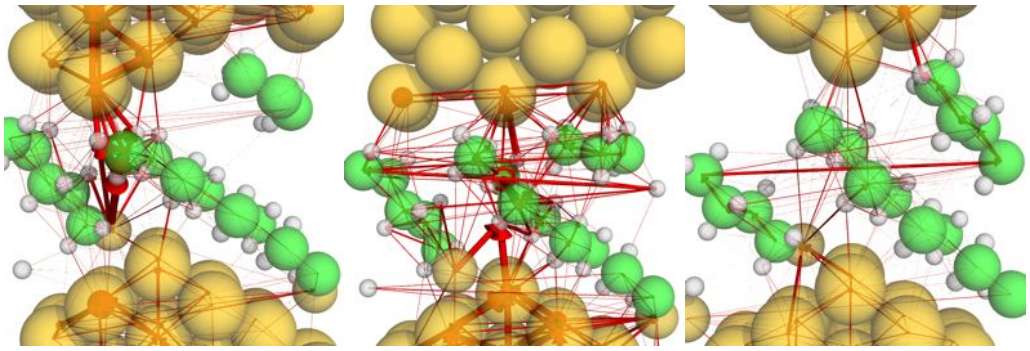

(a) "moved" *(b)* "flat" *(c)* "symmetric"

Figure 3.4: Current paths for setups a), b) and c) corresponding to Fig. 3.3, showing both intermolecule (a and b) and intramolecule (c) tunneling paths where the cross-sectional area of the arrows is proportional to the current density flowing upwards.

The resistance values calculated for OT molecules attached to different step edges vary by 1-2 orders of magnitude. Therefore, the attachment geometry of the Au-OT-Au junction is an important factor influencing the electron transmission through the electrodes. It should be emphasized that the structures that were calculated (figure 3.3) use the rearrangements of Au-atoms that achieve the lowest energy configuration, while in the actual experiments the shape of the junction is defined by the shape and relative arrangement of the NP and the electrode. Thus the resistance of the assembled device will largely depend on the amount of well-conducting molecules, which, in turn, is very sensitive to the structure and relative orientation of the surface defects. Nevertheless, in the experimental resistance histogram in figure 3.2 a), the resistances vary by nearly four orders of magnitude and therefore, in addition to the influence of the OT-Au configuration, it is likely that

other factors such as pin holes in the OT layer and shape of the NPs, where number of contacted molecules can vary greatly depending on the facetting of the NP, would influence the variation in measured resistances in this SAM based nanoelectrode platform.

3.2 Realization of highly reproducible molecular junctions in a nanoparticle-alkanedithiol-nanoelectrode bridge platform

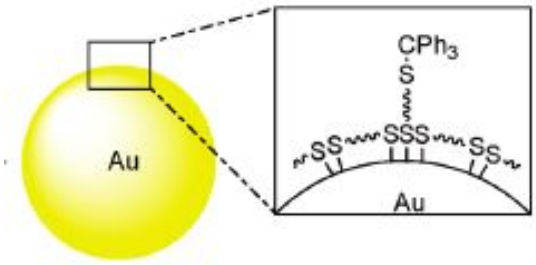

Figure 3.5: Schematic figure of thiol-stabilized gold nanoparticles with a coating of free standing protected alkanethiols. Reproduced from [55]

To enhance the reproducibility of the device it would be beneficial if it was possible to make chemical contacts to both electrodes, instead of just one as in the previous section. To able to do this the investigated molecule needs to have functional groups (for example thiols) in both ends that can chemisorb to the gold electrodes. Due to the reactiveness of the thiol groups some way to control that they bridge the gap and not only "backbite" to the same electrode is necessary. A chemical route for this has been developed [55] where they instead of coating the electrodes with molecules, build up stable AuNPs which are coated with α,ω-alkanedithiols whose outer ω-thiol is protected by a triphenylmethyl (trityl) group, a schematic is shown in Fig. 3.5. The surfaces of the AuNPs are also coated with a layer of 1,8-octanedithiol molecules, where both thiol groups have backbitten onto the nanoparticle surfaces and thus, the molecules are lying flat on the particle surface. The size of the protective groups makes it impossible for these groups to penetrate the layer of backbiting molecules.

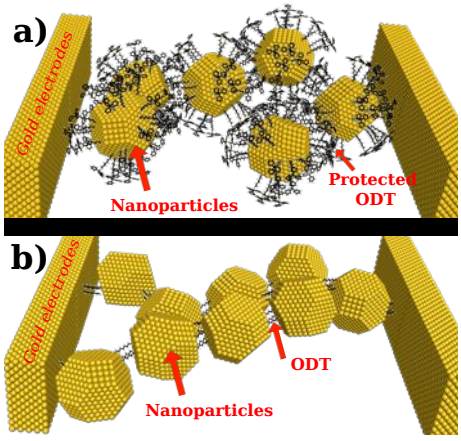

Figure 3.6: Schematic of how a nanoparticle-molecule-nanoparticle network between the electrodes can look: a) nanoparticles with protected molecules. b) nanoparticles with deprotected molecules that have chemisorb to two particles. In both cases stabilizing molecules on the surface are left out for clarity.

The functionalized AuNPs can be trapped in the nanogaps as in the previous case, the drawback here is that the diameter of the AuNPs is about 4-5 nm, hence it is necessary with several particles

to bridge the 20 nm gap. After the trapping, the ω-thiol can be deprotected via acid treatment and the now free thiol-group is small enough to penetrate the layer of backbiting molecules and chemisorb to the gold surface of an adjacent AuNP. Thus creating a covalently bonded network of AuNP-molecule-AuNP between the electrodes. Such possible networks for both protected and deprotected molecules are shown in Fig. 3.6.

Here we carry out theoretical calculations to investigate which atomic configurations that are probable in these junctions and to explain the increase in measured conductivity after deprotection of the molecules (Paper II). The experimental measurements after deprotection, shows the possiblity to do a large number of reproducible electrical measurements on a nanoparticle-nanoelectrode bridge platform.

In Fig. 3.7 , a scanning electron microscope image of trapped trityl-protected octanedithiol coated nano-particles is shown. As can be seen from the figure (and 3.6) several nanoparticles are necessary to bridge the gap, both in 2D and 3D networks, effects that have to be considered when interpreting the results.

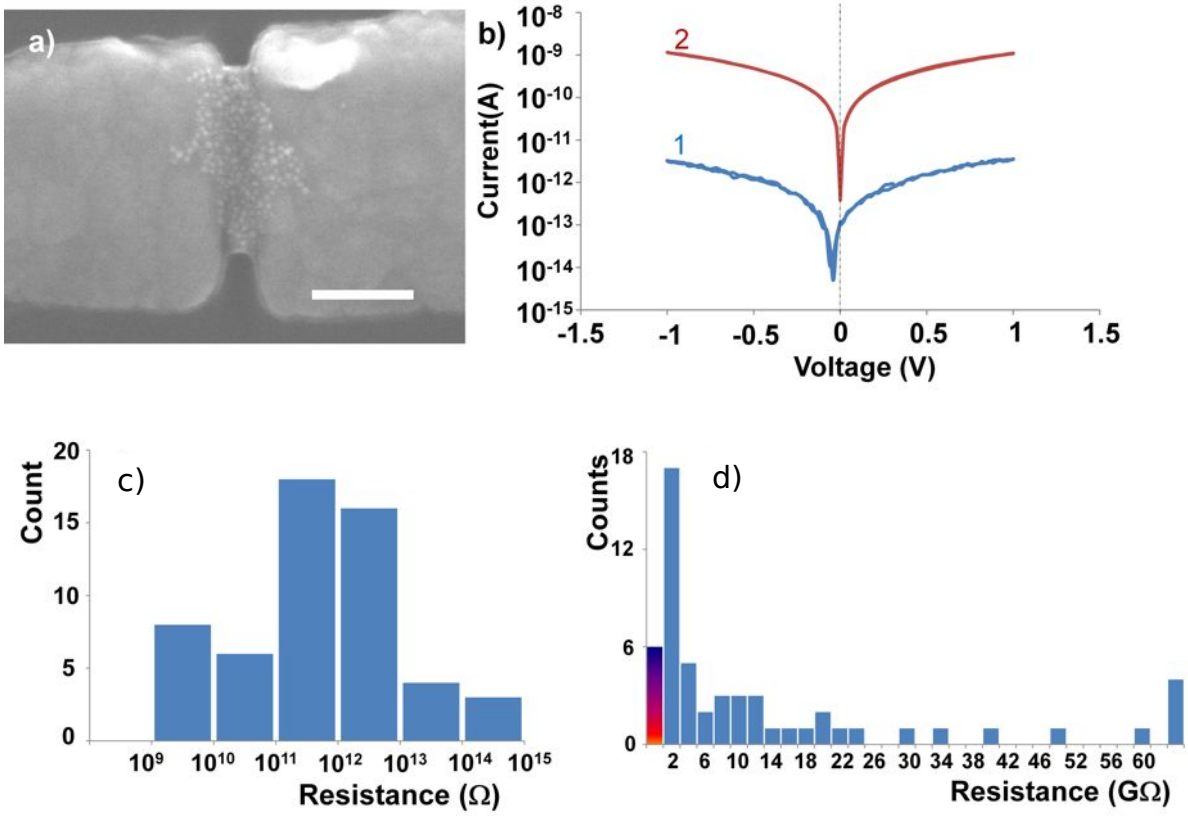

Figure 3.7: Top: a) Scanning electron image of ω-trityl protected 1,8-octanedithiol coated nanoparticles trapped in between nanoelectrode setup. b) Current-voltage (I-V) response of same device after trapping (1) and after removal of trityl protection groups from ω end of 1,8-octanedithiol (2). Bottom: c) log-normal resistance histogram of devices having ω-trityl protected 1,8-octanedithiol in nanoparticle-nanoelectrode bridge platform d) Linear scale resistance histogram (bin size=2 GΩ) of 1,8-octanedithiol in nanoparticle-nanoelectrode bridge platform after removal of trityl protecting group and establishing an chemisorbed metal-molecule junction.

The I-V curves for the two different junctions are shown in Fig. 3.7b where (1) corresponds to protected molecules and (2) to deprotected. Both devices demonstrates high resistance around 325 GΩ (1 GΩ) for (de)protected due to the large gap between the highest occupied molecular orbital (HOMO) and the lowest unoccupied molecular orbital (LUMO) of the octanedithiol molecule where the conduction mechanism is nonresonant tunneling with an exponential dependence on the tunneling distance[12]. The calculated distance between the two electrode surfaces spaced with the protected (deprotected) molecule is about 2.5 nm (1.5 nm). Comparing the I-V curves, (1)

shows more small-scale fluctuations compared to (2), this originate from that the junctions with protected molecules are not as stable since one end of the molecules is only physisorbed.

During removal of the trityl group, the outer ω-thiol is "free" and in the ideal case can attach to an adjacent AuNP, as the case shown in Fig.3.6, thus forming the covalently bond network with more stable junctions. An increase of conduction somewhere between 100 to 10^5 times can be seen as shown in the histogram in Fig. 3.8a, where the most prominent peak show an increase of 100 times. From the histograms in Fig. 3.7d and 3.7c, a similar behavior as for the I-V curves can be seen where junction with protected molecules shows a large spread in values, responsible for the large spread for the change in conduction during deprotection as well, whilst the junction with deprotected molecules shows a spread less than two orders of magnitude indicating that we have a device with stable chemical contacts and high reproducibility.

To get a better understanding of the molecular configurations in the junctions, we have modeled probable atomic configurations as shown in Fig. 3.8b.

For the single octanedithiol chain linked via the sulfur atoms in both ends to the gold surface (setup I in Fig. 3.8b), we have obtained a conductance of $30.5 \times 10^{-5} G_0$, ($G_0 = 2e2/h$) comparable to other theoretical studies[13] . In the case of ω-trityl protected 1,8-octanedithiol molecules (setup II in Fig. 3.8b), we have obtained a single molecule conductance 15 times lower as compared to the unprotected molecule. The decrease in conductance found here can be accounted for by the increase in distance between the gold electrodes from 15 Å to 18 Å to accommodate trityl groups. Assuming that the tunneling decay factor of the alkane chain is 0.7 $Å^{-1}$ [12, 52], would result in a decrease in conductance of around 10 times with this increase in distance. This can not explain the increase seen in experiments. Instead we tried the extreme where the protected molecules bind head to head, shown as IV in Fig. 3.8b. This configuration has a conductance of roughly 10^{-9} G_0, hence about 6 orders of magnitude smaller compared to the deprotected molecule. This increase is also outside what is observed in experiments, hence we have found the two extreme configurations for the protected molecule and the observed configuration should lie somewhere in between.

To investigate the configurations in between it is necessary to take the backbiting molecules into account since they might affect the distance between the electrodes when the protected molecules are clustering together. The results from this calculation (setup III Fig. 3.8b) shows a zero-bias conductance of 1.3×10^{-7} G_0, i.e. a decrease with three orders of magnitude compared to the octanedithiol chain. This is in good agreement with most observed values in the histogram plotted in Fig. 3.8a. Our results suggest that it is not the protection group itself that is responsible for the experimental measured decrease in conductance, but the increased distance between gold surfaces due to the size of the protection groups and the extra effective thickness added by the layer of molecules on the surface.

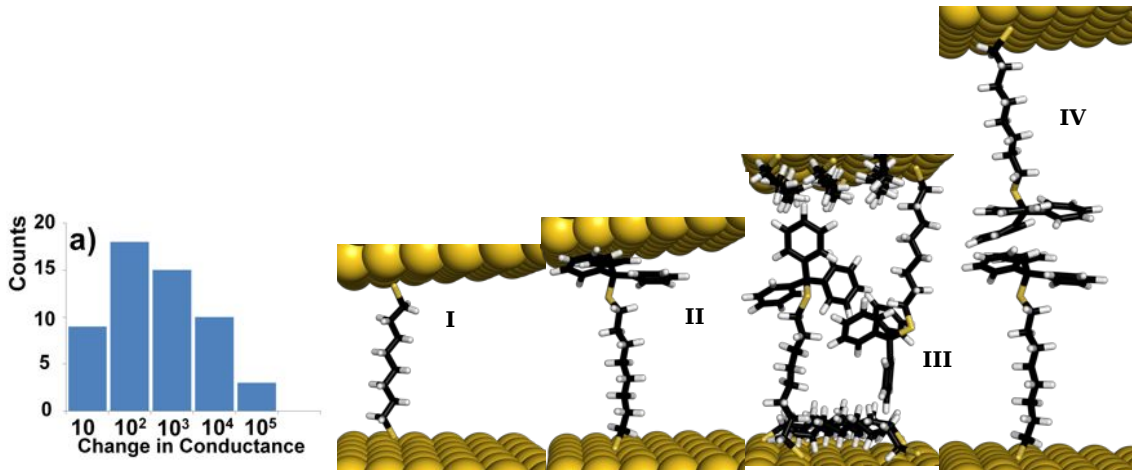

(a) Measured change *(b)* Atomic configurations

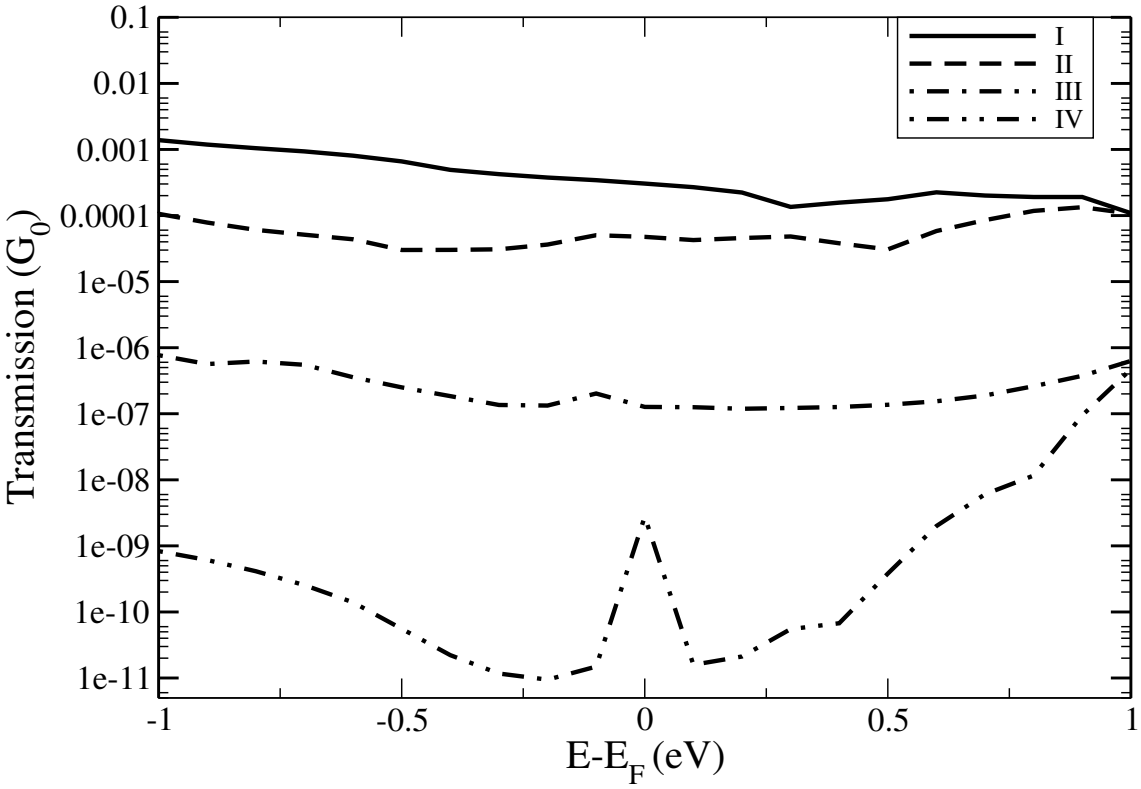

(c) Zero-bias transmission

Figure 3.8: a) Difference in conductivity of devices before and after removal of trityl protecting group, because of trityl protecting groups we have one physisorption junction at the end of molecule and after removal of trityl protecting group chemisorbed junctions established at both end of molecules b) Atomic configuration considered in theoretical simulation I) 1, 8-octanedithiol chemisorbed at two nearby gold surfaces II) ω-trityl protected 1, 8-octanedithiol chemisorbed at one end and physisorbed at other end. III) ω-trityl protected 1, 8-octanedithiol attached to the both gold surfaces in presence of surface layer of backbiting 1,8-octanedithiol on both gold surfaces IV) ω-trityl protected 1, 8-octanedithiol attached to both electrode surface at maximum separation. c) Zero-bias transmission for the four considered setups

3.3 Vibrational signatures in inelastic electron tunneling spectroscopy from short molecule-nanoparticle chains trapped in versatile nanoelectrodes

To probe the structure of molecules in the nanoscale junction considered in the previous sections and prove that we can identify the octanedithiol molecule in junction, inelastic electron tunneling spectroscopy (IETS)[56, 57] measurements have been done, where molecules can be identified by their vibrational signature. The main setup considered is the octanedithiol covalently bond to gold electrodes.

In Fig. 3.9 the I-V curve for the measured junction together with the first (dI/dV) and second (d^2I/dV^2) derivatives of the current are shown. These measurements were performed at liquid He temperatures. When the bias voltage is increased, no current flows until the voltage exceeds 0.15 V. The suppression of the current until this threshold voltage is due to Coulomb blockade[58], this effect is more clearly seen in the first derivative of the current (3.9 b)). For bias voltages larger than the threshold a non-linear increase of the current can be observed, indicating that we have inelastic processes opening more conduction channels through vibrations in the molecules. The excitation of a new conduction channel is clearly seen in the dI/dV (3.9 b)) as steps. The steps in the dI/dV show up as clear peaks in the d^2I/dV^2 (Fig. 3.9 c)), and it can be noted that both the dI/dV and the d^2I/dV^2 are asymmetric especially for higher voltages. This can be expected since we have networks of molecules with parallel chains which can give different current paths for negative and positive bias voltage.

To understand the signatures observed in the d^2I/dV^2 we have modeled both the elastic and inelastic conductance through the Au-molecule-Au junction. The elastic conductance was calculated as in the previous sections, the inelastic current was calculated through the lowest order expansion (LOE) method described in Section 2.5.3. To apply LOE the system needs to have a weak electron-phonon coupling and the density of states close to Fermi energy should vary slowly. This can be justified by the transmission spectra in Fig. 3.10 which has no sharp peaks close to the Fermi energy, hence the conductance is almost bias independent. It has also been shown that less then 3% of the electrons undergo inelastic scattering for alkanethiols[59].

The calculated IETS for a ODT molecule sandwiched between two gold surfaces is shown in Fig. 3.11 together with the most important vibrational modes of the molecule. The vibrational modes that have most influence on the current is Au-S stretch ($\omega \sim 40$ meV), C-S stretch ($\omega \sim 84$ meV), CH_2 twist ($\omega \sim 109$ meV) and two C-C stretch ($\omega \sim 122$ meV and $\omega \sim 142$ meV). In 3.11 a)

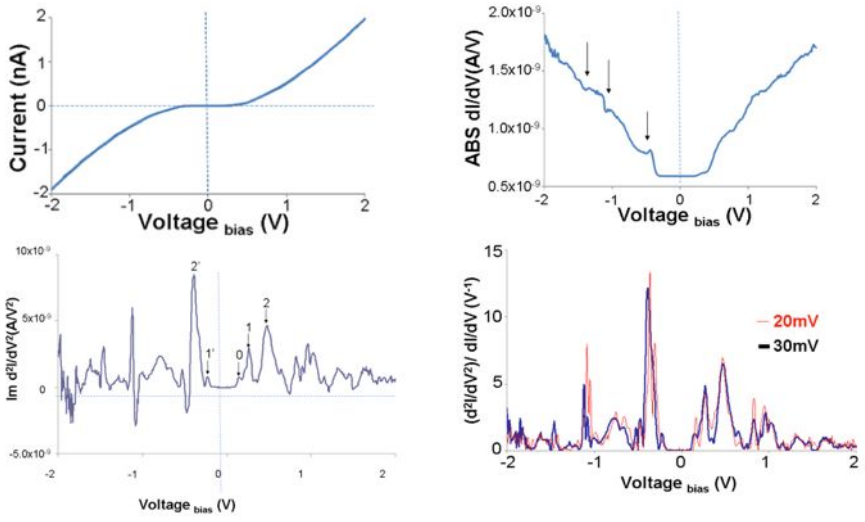

Figure 3.9: Electrical characterisation of the nanoelectrode-molecule-nanoparticle junction. a) Measurement of current-voltage characteristics. b) Module of the dI/dV vs. V. c) Im (d^2I/dV^2) vs. V. The peak energies of the low energy peaks are: $E_0 = 150$ meV, $E_1 = 250$ meV, $E_2 = 450$ meV, $E_{1'} = -240$ meV, $E_{2'} = -380$ meV. d) Inelastic electron tunnelling spectrum $(d^2I/dV^2)/(dI/dV)$ vs. V.

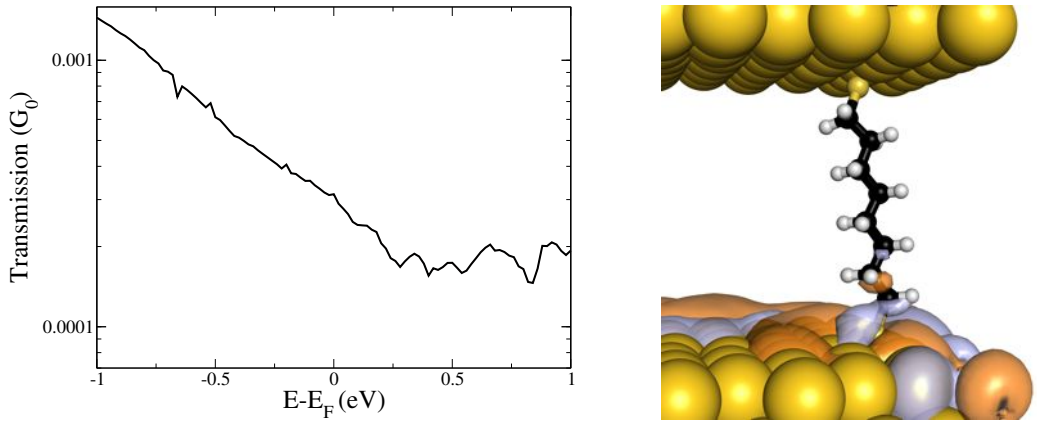

Figure 3.10: (a) Zero-bias transmission for ODT molecule sandwiched between two gold electrodes. (b) The main conduction channel (from bottom electrode to top) for the octanedithiol molecule

also the IETS for the trityl-protected molecule is shown in dashed as a comparison, where it is possible to see that the low-bias peaks appear at similar voltages, hence corresponding to similar modes, but with different intensities also the higher C-H stretch mode ($\omega \sim 350$ meV) is much more pronounced for the protected molecule, hence it should be possible to separate the two molecules from their signatures. The low-bias peaks corresponding to the Au-S stretch and C-S stretch are the dominating in the spectra. This can be expected since vibrations close to where the low bias conduction channel has electron density should give peaks of highest intensity[60]. As can be seen from Fig. 3.10b, the main conduction channel is localized close to the terminal sulfur atom.

Since at least 4 ODT functionalized NPs are need to bridge the gap, the measured response corresponds to a chain of N molecules in series, i.e a sum of resistances. Therefore to relate the calculated response of a single molecule the voltage scale has to be multiplied by N to correspond to the measured spectra. This is justified if we can assume that all junctions are equal in resistance, hence the voltage drop over each junction is equal.

In the following we use a model that is not just scaling the voltage scale to explain the experiments, but also includes the measured Coulomb blockade. As input to the model the most important vibrations modes and their electron-phonon coupling estimated from Fig. 3.11a were used. A more depth description of the carrier transport model related to the vibrational states of the molecules in such a NP-molecule chain including the activation energy related to the Coulomb energy of the NPs is found in the SI of Paper III. The total resistance used in the model will be the sum of several chains of resistances in series and parallel, where the smallest number of resistances in series is 4 (necessary to bridge the gap) and largest number is 14. A sketch of such a network is shown in Fig. 3.12 a).

The linear combination of the IETS spectrum of all chains from the model is then fitted to the experimental IETS spectrum, since the asymmetry of the measured curves the fitting is carried out separately for negative and positive bias. The resulting curve is shown in 3.12b, where the parameters of the fit is noted above the curve (a is the total number of chains for each length of resistances in series (4-14)). The experimental peaks at low energies corresponds well to the fitted results, higher energy peaks are much broader and contains vibrations from several modes since low energy modes from longer chains will appear at similar energies as high energy modes from short chains producing broad peaks, hard to resolve. The peak 1 in the experimental spectra (Fig. 3.9c) is estimated to contain the Au-S signal from NP-molecule chains containing 5, 6 and 7 molecule junctions. The experimental peaks 2 and 2' have a FWHM of 110-140 meV meaning that they contain a number of peaks, but still it can be estimated that the main contribution should be from the C-S stretch mode from NP-molecule chains of 5, 6 and 7 molecule junctions. These estimations shows that the strongest contribution to the experimental spectra should come from chain containing 5, 6 and 7 molecule junctions, which agree well with the estimation that at least 4 molecule junctions are needed to bridge the gap between the nano-electrodes.

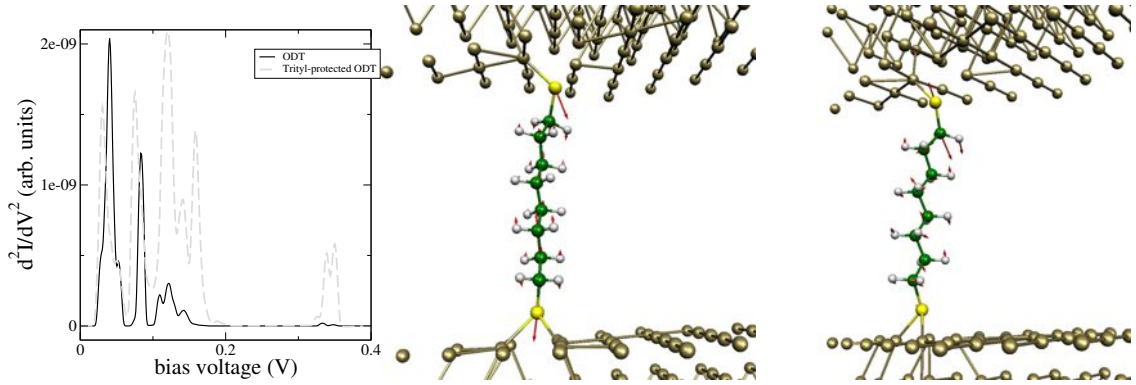

(a) Inelastic spectra *(b)* Au-S stretch (40 meV) *(c)* C-S stretch (84 meV)

(d) CH2 twist (109 meV) *(e)* C-C stretch (122 meV) *(f)* C-C stretch (142 meV)

Figure 3.11: (a) Inelastic spectra (d^2I/dV^2) for a ODT molecule between gold electrodes. (b)-(f) The five "most" important vibrations mode of the molecule. Au-S stretch, C-S stretch, "CH2 wagging" and two different C-C stretch

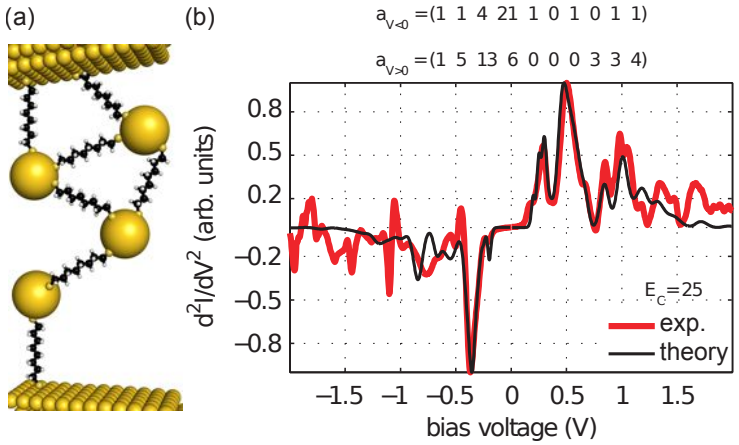

Figure 3.12: (a) Cartoon of one molecular chain in the nanogap. Chain consists of a number N molecular junctions and $N-1$ NPs linking the molecules together. (b) Calculated IETS using the modeling described fitting (least square) the number of chains with $N = 4, 5, \ldots, 14$ molecular junctions. For the calculations we have used the vibrational modes $\omega_n \in \{40,\ 84, 109,\ 122,\ 142\}$ meV with corresponding coupling to the tunneling electrons $\lambda_n^2 \in 1.5625 \cdot \{4.4\ 3.7,\ 0.6,\ 0.5,\ 0.1\}$ in units of the elastic tunnel current. The activation energy is set to $E_C = 25$ meV, while the temperature is set to $T = 20$ K for the sake of broadening. The experimental curve has been Lorentzian broadened by 10 meV.

4. Conclusions and outlook

In this study a nanoparticle bridge platform was assessed for molecular electronics measurements. It is a platform, that can be used for stable and reproducible measurements, further it presents several advantages over other testbeds, such as simplicity and ability to perform measurements in ambient conditions. There still exist several difficulties connected to it in need for further investigations.

Simulations show that structural irregularities at the electrode interface can lead to a significant variation of molecular film conductance. In the case of insulating molecules (like octanethiols(OT)), the crucial parameter is the effective molecular film thickness. It should be emphasized that surface defects in close vicinity to 'tails' (CH2 chains of OT) facilitate charge transport as compared to perfect tight film packing on a flat surface where such tails do not come into direct contact with the metal of the electrode. This leads to an increased electron tunneling rate from metal through the molecular film on the defect containing surfaces.

To enhance the reproducibility of the platform, the physisorbed metal-molecule junction in the case of OT-molecules can be replaced by a chemisorbed junction with ODT-molecules. To form the chemisorbed junctions, nanoparticles coated with molecules having two functional groups are necessary where the outer functional group needs to be protected during trapping of the particles in the nanogap. The nanoparticles with the protected molecules are physisorbed in the junction in a number of different molecular configurations, giving rise to a broad resistance histogram. After deprotection the free functional group can chemisorb to the gold surface and make stable contacts, resulting in a narrow resistance histogram. Simulations show that the decreased resistance during deprotection is not due to the removal of the protection group, but to a shorter molecular bridge, giving a smaller tunneling barrier for the electron through the gap between the particles.

To identify the molecules in the nanogap, the method of IETS can be used. Fitting the calculated theoretical spectra to the measured response, peaks characteristic for the ODT molecule can be identified. Due to the size of the nanoparticles, a chain of junctions between nanoparticles/nanoelectrodes containing assemblies of molecules are needed. We can conclude that the main contribution from the measured response should originate from chains with 5, 6 and 7 of such junctions.

Thus we have shown that the nanoparticle-molecule-nanoelectrode bridge platform can be used for fundamental physical measurements. Moreover, since the platform easily can be transported and is built by conventional micro-and nano-structuring tools, it opens applications with few molecule electronics and sensorics to a wider field of applications in medicine, nano- and biotechnology. To proceed the next thing is to investigate more suitable molecules, that can act as a sensors, switches and other interesting components.

5. Acknowledgement

First of all I would like to thank my supervisor Prof. Rajeev Ahuja who made it possible for me to start my PhD studies in the Division of Materials Theory. Secondly I would like to thank Prof. Jan Isberg, my co-supervisor who has introduced me to the very interesting field of diamond electronics. We would also like to acknowledge Carl Tryggers Stiftelse for Vetenskaplig Forskning, the Swedish Energy Agency and the Uppsala University Unimolecular Electronics Center (U3MEC) for financial support.

I am also most grateful to Anton Grigoriev, who been my guide through the field of molecular electronics and the methods used here. And also for his help reading and revising manuscripts and this thesis.

I would like to thank Henrik Ottoson, Klaus Leifer, Jonas Fransson, Hassan Jafri, Tobias Blom and Andreas Wallner, for all the work and fruitful discussions around the nanoparticle platform investigated here. I would also like to thank all other people involved in the U3MEC for interesting discussions during our meetings and for trying to teach me all the chemistry needed for the work here. Also many thanks to Magnus Paulsson for the introduction and help both using and extending the inelastica code. Thanks also goes to everybody at the Division of Material Theory for making us an outstanding research group, and especially to Oscar, Jonas, Peter, Lisa, Anders, Petros, Cecilia, Fredrik et. al for all interesting lunch table discussions.

Finally I would like to thank my family, most of all Elin and Algot, for their love and always being there for me.

References

[1] *http://www.intel.com/content/www/us/en/silicon-innovations/moores-law-embedded-technology.html* (2011).

[2] G. E. Moore, *Int. El. Devices Meet.* **21**, 11 (1975).

[3] G. E. Moore, *Electronics* **38**, 114 (1965).

[4] *http://news.cnet.com/2100-1008-5112061.html* (2011).

[5] J. R. Heath and M. A. Ratner, *Phys. Today* **56**, 43 (2003).

[6] A. Aviram, *Chem. Phys. Lett.* **29**, 277 (1974).

[7] A. Aviram, *J. Am. Chem. Soc.* **110**, 5687 (1988).

[8] A. R. Brown, A. Pomp, C. M. Hart, and D. M. de Leeuw, *Science* **270**, 972 (1995).

[9] K. M. Roth, N. Dontha, R. B. Dabke, D. T. Gryko, C. Clausen, J. S. Lindsey, D. F. Bocian, and W. G. Kuhr, *J. Vac. Sci. Technol. B* **18**, 2359 (2000).

[10] K. Phoa, J. B. Neaton, and V. Subramanian, *Nano Lett.* **9**, 3225 (2009).

[11] M. A. Reed, *Science* **278**, 252 (1997).

[12] H. B. Akkerman and B. de Boer, *J. Phys.-Condens. Mat.* **20**, 013001 (2007).

[13] M. Paulsson, C. Krag, T. Frederiksen, and M. Brandbyge, *Nano Lett.* **9**, 117 (2009).

[14] A. Sen and C.-c. Kaun, *Acs Nano* **4**, 6404 (2010).

[15] W. Sheng, Z. Y. Li, Z. Y. Ning, Z. H. Zhang, Z. Q. Yang, and H. Guo, *J. Chem. Phys.* **131**, 244712 (2009).

[16] C. Li, I. Pobelov, T. Wandlowski, A. Bagrets, A. Arnold, and F. Evers, *J. Am. Chem. Soc.* **130**, 318 (2008).

[17] T. Frederiksen, C. Munuera, C. Ocal, M. Brandbyge, M. Paulsson, D. Sanchez-Portal, and A. Arnau, *Acs Nano* **3**, 2073 (2009).

[18] G. C. Solomon, C. Herrmann, and M. A. Ratner, *Molecular Electronic Junction Transport: Some Pathways and Some Ideas* , Topics in Current Chemistry, Springer Berlin Heidelberg, Berlin, Heidelberg, 2011.

[19] J. Liao, J. S. Agustsson, S. Wu, C. Schönenberger, M. Calame, Y. Leroux, M. Mayor, O. Jeannin, Y.-F. Ran, S.-X. Liu, and S. Decurtins, *Nano Lett.* **10**, 759 (2010).

[20] T. Blom, K. Welch, M. Strømme, E. Coronel, and K. Leifer, *Nanotechnology* **18**, 285301 (2007).

[21] J. M. Soler, E. Artacho, J. D. Gale, A. Garcia, J. Junquera, P. Ordejon, and D. Sánchez-Portal, *J. Phys.-Condens. Mat.* **14**, 2745 (2002).

[22] M. Born, *Ann. Phys.* (1927).

[23] P. Hohenberg and W. Kohn, *Phys. Rev.* **136**, B864 (1964).

[24] W. Kohn and L. J. Sham, *Phys. Rev.* **140**, A1133 (1965).

[25] C. Arhammar, *Atomistic modelling of functional solid oxides for industrial applications*, PhD thesis, Department of Materials Science, Royal Insitute of Technology, Stockholm, Sweden, 2011.

[26] J. P. Perdew and Y. Wang, *Phys. Rev. B* **45**, 13244 (1992).

[27] J. P. Perdew, K. Burke, and M. Ernzerhof, *Phys. Rev. Lett.* **77**, 3865 (1996).

[28] E. Artacho, E. Anglada, O. Diéguez, J. D. Gale, A. García, J. Junquera, R. M. Martin, P. Ordejon, J. M. Pruneda, D. Sanchez-Portal, and J. M. Soler, *J. Phys.-Condens. Mat.* **20**, 064208 (2008).

[29] N. Troullier and J. L. Martins, *Phys. Rev. B* **43**, 1993 (1991).

[30] D. R. Hamann, M. Schlüter, and C. Chiang, *Phys. Rev. Lett.* **43**, 1494 (1979).

[31] L. Kleinman and D. M. Bylander, *Phys. Rev. Lett.* **48**, 1425 (1982).

[32] J. Junquera, O. Paz, D. Sánchez-Portal, and E. Artacho, *Phys. Rev. B* **64**, 235111 (2001).

[33] E. Anglada, J. M. Soler, J. Junquera, and E. Artacho, *Phys. Rev. B* **66**, 205101 (2002).
[34] E. Artacho, D. Sánchez-Portal, P. Ordejón, A. García, and J. M. Soler, *Phys. Status Solidi B* **215**, 809 (1999).
[35] S. Baroni, S. de Gironcoli, and A. Dal Corso, *Rev. Mod. Phys.* **73**, 515 (2001).
[36] T. Frederiksen, M. Paulsson, M. Brandbyge, and A.-P. Jauho, *Phys. Rev. B* **75**, 205413 (2007).
[37] M. Brandbyge, J.-L. Mozos, P. Ordejón, J. Taylor, and K. Stokbro, *Phys. Rev. B* **65**, 165401 (2002).
[38] M. Di Ventra, *Electrical Transport in Nanoscale Systems*, Cambridge University Press, 2008.
[39] T. Frederiksen, M. Brandbyge, N. Lorente, and A.-P. Jauho, *Phys. Rev. Lett.* **93** (2004).
[40] T. Frederiksen, M. Brandbyge, A.-P. Jauho, and N. Lorente, *J. Comp. Elec.* **3**, 423 (2004).
[41] M. Paulsson and T. Frederiksen, *J. Phys. Conf. Ser.* **35**, 247 (2006).
[42] M. Paulsson, T. Frederiksen, and M. Brandbyge, *Phys. Rev. B* **72**, 201101 (2005).
[43] M. Paulsson, T. Frederiksen, and M. Brandbyge, *Nano Letters* **6**, 258 (2006).
[44] T. Frederiksen, N. Lorente, M. Paulsson, and M. Brandbyge, *Phys. Rev. B* **75** (2007).
[45] M. Strange, C. Rostgaard, H. Häkkinen, and K. S. Thygesen, *Phys. Rev. B* **83**, 115108 (2011).
[46] C. Toher and S. Sanvito, *Phys. Rev. Lett.* **99** (2007).
[47] C. Toher, A. Filippetti, S. Sanvito, and K. Burke, *Phys. Rev. Lett.* **95** (2005).
[48] A. R. Rocha, V. M. García-suárez, S. W. Bailey, C. J. Lambert, J. Ferrer, and S. Sanvito, *Nat. Mat.* **4**, 335 (2005).
[49] M. Strange, I. S. Kristensen, K. S. Thygesen, and K. W. Jacobsen, *J. Chem. Phys.* **128**, 114714 (2008).
[50] S.-H. Ke, H. U. Baranger, and W. Yang, *J. Chem. Phys.* **127**, 144107 (2007).
[51] C. Herrmann, G. C. Solomon, J. E. Subotnik, V. Mujica, and M. A. Ratner, *J. Chem. Phys.* **132**, 024103 (2010).
[52] W. Wang and T. Lee, Intrinsic electronic conduction mechanisms in self-assembled monolayers, in *Introducing Molecular Electronics*, edited by G. Cunberti, G. Fagas, and K. Richter, p. 275, Springer, 2005.
[53] G. Binnig, H. Rohrer, and C. Gerber, *Surf. Sci. Lett.* (1983).
[54] C. George, H. Yoshida, W. A. Goddard, S. S. Jang, and Y.-H. Kim, *J. Phys. Chem. B* **112**, 14888 (2008).
[55] A. Wallner, S. H. M. Jafri, T. Blom, A. Gogoll, K. Leifer, J. Baumgartner, and H. Ottosson, *Langmuir* **27**, 9057 (2011).
[56] M. A. Reed, *Mat. Today* **11**, 46 (2008).
[57] J. Lambe and R. Jaklevic, *Phys. Rev.* **165**, 821 (1968).
[58] S. I. Khondaker, K. Luo, and Z. Yao, *Nanotechnology* **21**, 095204 (2010).
[59] N. Okabayashi, Y. Konda, and T. Komeda, *Phys. Rev. Lett.* **100** (2008).
[60] G. C. Solomon, A. Gagliardi, A. Pecchia, T. Frauenheim, A. Di Carlo, J. R. Reimers, and N. S. Hush, *J. Chem. Phys.* **124**, 094704 (2006).